Experimental investigation of recoating forces in sand binder jetting

Raphael Burger, Maximilian Mack, Veikka Innanen, Elodie Donval, Matti Schneider, Philipp Lechner, Wolfram Volk, Daniel Günther

Angaben zur Veröffentlichung / Publication details:

Burger, Raphael, Maximilian Mack, Veikka Innanen, Elodie Donval, Matti Schneider, Philipp Lechner, Wolfram Volk, and Daniel Günther. 2026. "Experimental investigation of recoating forces in sand binder jetting." *Powder Technology* 480: 122631. https://doi.org/10.1016/j.powtec.2026.122631.

Powder Technology 480 (2026) 122631

Contents lists available at ScienceDirect

Powder Technology

journal homepage: www.journals.elsevier.com/powder-technology

Experimental investigation of recoating forces in sand binder jetting

Raphael Burger [a,b,*], Maximilian Mack [a,b], Veikka Innanen [a,b], Elodie Donval [c,f], Matti Schneider [c,d], Philipp Lechner [e], Wolfram Volk [a,b], Daniel Günther [a,b]

[a] Fraunhofer Institute for Casting, Composite and Processing Technology, Garching, Germany
[b] Chair of Metal Forming and Casting, Technical University of Munich, Germany
[c] Institute of Engineering Mathematics, University of Duisburg–Essen, Germany
[d] Fraunhofer Institute for Industrial Mathematics ITWM, Kaiserslautern, Germany
[e] Institute of Materials Resource Management, University of Augsburg, Germany
[f] CNRS, Univ. Grenoble Alpes, Grenoble INP, 3SR, Grenoble, France

HIGHLIGHTS

- First experimental quantification of recoating forces in sand binder jetting.
- Dual load cell system records tangential and normal forces simultaneously.
- Blade angles of 88° - 90° minimize tangential and normal recoating forces.
- Roller forces stabilize with increasing rotational speed.
- Force Differences at part boundaries are higher for rollers than blades.

GRAPHICAL ABSTRACT

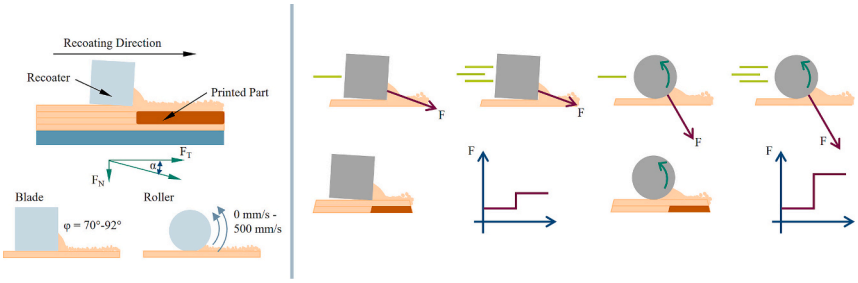

ARTICLE INFO

Keywords:
Recoating forces
Sand binder jetting
Layer shifting
Geometric uncertainties
Process optimization

ABSTRACT

Additive manufacturing of sand molds using binder jetting enables production of geometrically complex castings. Process parameters during recoating significantly affect and impair part quality. While recoating forces have been studied extensively through simulations for metal powder bed fusion, experimental quantification for sand binder jetting is lacking. The transferability of existing models to sand systems with larger, irregular particles remains unclear.

This work presents systematic experimental quantification of both tangential and normal recoating forces in sand binder jetting. A dual load cell measurement system was developed to simultaneously capture both force components during recoating. The two most common industrial recoater geometries (blades and rollers) were investigated. Blade angles (70°–92°), roller circumferential speeds (0–500 mm/s), and recoating velocities (100 mm/s and 300 mm/s) were systematically studied using GS14RP sand. Additionally, force differences at transitions between unprinted and printed areas were examined.

Blade recoaters showed minimum forces at angles of 88°–90°, while 92° blade angle produced sharply increased forces and a visible displacement of the printed region in the powder bed. Roller recoaters achieved stable conditions at circumferential speeds above 200 mm/s. Blade recoaters exhibited decreasing forces with increasing recoating velocity, whereas roller recoaters showed the opposite trend. Force differences at part boundaries were significantly higher for rollers than for blades, particularly at elevated recoating velocities.

* Corresponding author at: Fraunhofer Institute for Casting, Composite and Processing Technology, Garching, Germany.
E-mail address: raphael.burger@igcv.fraunhofer.de (R. Burger).

https://doi.org/10.1016/j.powtec.2026.122631
Received 9 March 2026; Received in revised form 21 April 2026; Accepted 2 May 2026
Available online 9 May 2026

This study provides experimental data for recoating forces in sand binder jetting, complementing particle-scale force chain frameworks from the DEM literature and establishing a foundation for future process optimization. From our results, we identified the configurations that minimize the recoating forces.

1. Introduction

The industrial application of sand binder jetting to produce lost geometries for sand cores and sand molds has been increasing recently. In foundry technology sand cores and sand molds are used to produce lost geometries. Additive manufacturing widely eliminates geometric restrictions and enables the production of complex part geometries [1]. While direct 3D printing with laser powder bed fusion (L-PBF) is increasingly being to produce the final part, 3D printing with sand allows printing sand cores for lost geometries and entire molds. This allows for creating casted parts of complex shape and the efficient use of foundry resources. Sand binder jetting is divided into recoating, printing and lowering. These steps are illustrated in Fig. 1.

During the layer-by-layer process, sand is deposited into the cavity created by lowering the build platform. To create a homogeneous surface and to compact the powder bed, a sufficient amount of sand needs to be applied and smoothed in the recoating step before binder is selectively printed. Here, the excess sand required to ensure process reliability is referred to as powder pile. For economical production, the steps in Fig. 1 must be carried out as quickly as possible. The major limitation comes from the recoating step, where recoating velocity cannot be increased arbitrarily without affecting part quality [2].

A central quality problem during recoating is the displacement of previously printed layers, referred to as layer shifting. A typical cross-section is shown in Fig. 2. The layer wise displacement accumulates over multiple layers and leads to a visible curvature of the part surface. These effects occur in the lowest layers or after unprinted layer sections and usually affect small, printed areas of less than 2 cm^2. Small, narrow structures with expansions perpendicular to the recoating direction might also be affected.

Consequences of shifted layers are uncertainties on the final part geometry, reduced surface quality and reduced quality of the casted part [3]. The recoater geometry, the recoating velocity and the layer thickness are reported as relevant parameters for the occurrence of layer shifting, affecting the mass flow in the powder pile, the location of the shear band and the forces exerted on the powder bed [2,4,5]. Several studies attribute the observed displacement to force arcs that form between sand grains in front of the recoater and to the resulting force chains that transmit the recoating force into the powder bed [4–6]. The reported relationships between process parameters and layer shifting are not consistent across studies: higher recoating speed is usually associated with more severe layer shifting. Chen et al. [7,8] find that higher recoating speed may lead to better surface quality than a lower recoating speed depending on process parameters. This indicates that the influence of recoating parameters on layer shifting is not yet fully understood and that further experimental data on the underlying forces are needed.

The mechanisms by which recoating parameters affect the powder bed have been studied predominantly through DEM simulations on the particle scale, mostly in the context of metal powder bed fusion. These simulations describe phenomena that cannot be directly observed in experiments and will provide the conceptual framework for interpreting macroscopic recoating forces.

Several DEM studies show that primally the recoater geometry and the gap between recoater and powder layer, i.e. the layer thickness, determine both the magnitude and the direction of the resulting forces and influence the particle flow in the powder pile in front of the recoater [9–12]. Tangential forces are reported to dominate with blade recoaters, while roller recoaters induce additional vertical force components and are more sensitive to layer thickness [9,13,14]. The recoating velocity and the roller circumferential speed affect particle flow and packing density in a non-monotonic way. Lifting and rearrangement of particles by counter-rotating rollers can increase density at moderate speeds, while excessive speeds lead to dilatation, looser packing and unstable particle flow [4,6,9,13,15]. Phua et al. [15] further report that higher recoating velocities increase the kinetic energy of the powder pile and improve convective particle flow. Beyond the resulting forces, the geometry of the recoater also affects the surface quality of the deposited layer. Rollers are reported to produce lower surface roughness and higher particle volume fractions than blades, which is attributed to their larger contact area [16].

A central concept in these simulations is the formation of force chains between particles in the powder pile. In the simulation models, the recoating force is transmitted through the powder bed via interconnected contact networks, see Fig. 3, in which load-bearing particle chains form, compress and collapse as the recoater advances [6,9,11,17]. Inclined and round blade geometries are reported to generate shorter and more numerous force chains in the compact region, while rotating rollers continuously break these chains through their rotation. This is also visible as fluctuations in the simulated force signals [6,9]. The relationship between force chain dynamics and microscopic contact behavior has been studied in granular mechanics. Liu et al. [18] show that force chain buckling under deviatoric loading is closely linked to contact sliding. Sliding contacts are strongly influenced by force chain instability rather than being part of the chains themselves. Chen et al. [6] further distinguish between static and dynamic wall effects, where the recoater acts as a moving boundary that disrupts the contact network at higher recoating velocities [7]. When the powder bed is described as a granular continuum rather than as discrete particles, shear failure can be modelled with criteria such as the Mohr-Coulomb model [19,20], although such continuum descriptions do not resolve the individual contact events of the DEM picture.

The framework concept of force arcs, force chains, contact network dynamics and shear failure are described on the particle scale and within simulation models, where individual contact forces are accessible as model output. They are not directly observable in experiments but

Fig. 1. Process steps of the sand binder jetting process (Erhard et al. [1]).

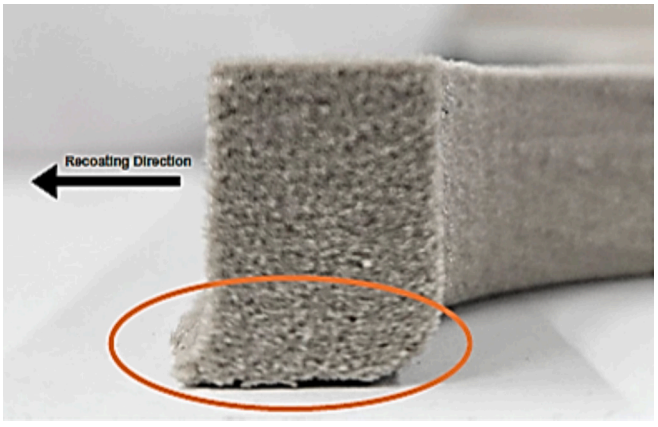

Fig. 2. Displaced layers of a printed part during the recoating step. The arrow indicates the recoating direction.

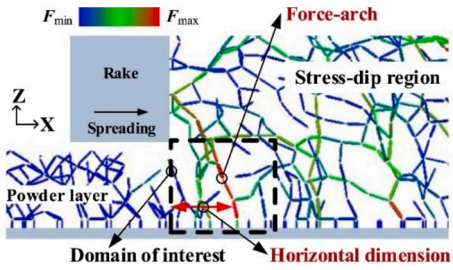

Fig. 3. Force arcs formed by dynamic wall effect (Chen et al. [21]).

manifest on the macroscopic scale as forces between recoater and powder bed [5,6].

Compared to the simulation literature on metal PBF, experimental studies that directly measure recoating forces in binder jetting are sparse. The few available experimental works focus on indirect quality indicators rather than on direct force measurements. Maximenko et al. [22] combine experiments with modelling and show that the localized flow during recoating extends over at least 6 to 10 particle diameters and that the reduced flowability of thin layers is attributed to the formation of stress chains under load. The deformation angle of thin-walled green bodies is inversely proportional to the thickness of the deposited layer and directly proportional to the square root of the thickness of the powder layer removed during recoating. A direct force measurement is provided by Parteli and Pöschel [17]. They simulate polymer PBF (PA, $D_{50} = 60$ µm) with a counter-rotating roller and report that both horizontal and vertical force components acting on a printed part fluctuate strongly in time, the vertical component varying by almost one order of magnitude as the roller passes over the part, see Fig. 4. They attribute these fluctuations to the formation of force chains in the powder packing. Miyanaji et al. [23] show that binder saturation and in-process drying is critical for green part quality, with insufficient drying time leading to layer shearing defects. A more direct experimental approach has recently been presented by Brika and Brailovski [24], who developed a dedicated test apparatus to measure the horizontal spreading forces, powder bed density and surface uniformity during recoating. Beyond these isolated studies, the role of the recoater geometry for the overall powder spreading quality is also recognized [25]. However, no equivalent experimental characterization has been reported for sand binder jetting.

The transfer of the simulation results from metal PBF to sand binder jetting is limited by differences in particle and process characteristics. Sand particles have a mean diameter of $D_{50} = 135$ µm, substantially larger than typical metal powders with D_{50} around 40 µm. Furthermore,

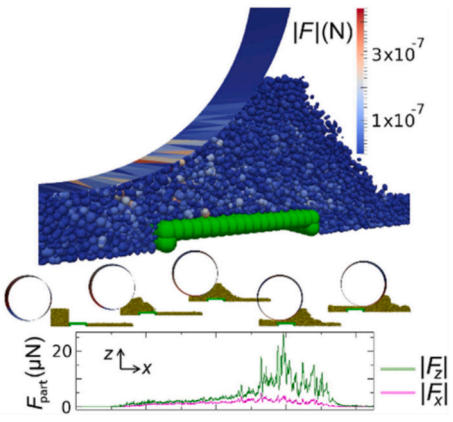

Fig. 4. Force magnitudes of total recoating forces while recoating over a sample part (green) (Parteli et al. [17]). (For interpretation of the references to colour in this figure legend, the reader is referred to the web version of this article.)

they are irregular rather than spherical. Cohesion effects, which are dominant in fine metal powders, are negligible in sand. The application mechanisms in commercial sand binder jetting systems also differ from those used in many of the cited PBF studies. Dedicated work on sand binder jetting itself is limited to a small number of simulation studies. Donval et al. [26] provide a first simulation basis by modelling the layer-by-layer application of sand through a directed contraction of a unit cell. Their model does not address the recoating forces themselves. Li and Yan. [27] develop a CFD-DEM coupling model for binder jetting and show that printed layers are displaced under combined normal and shear forces during recoating. Longer drying times reduce the shifting distance by allowing the binder to stiffen. Their model uses fine metal powders and a thermally activated methacrylate binder, so the transfer of these results to sand systems remains unclear.

The literature on recoating in binder jetting is dominated by particle-scale simulations for metal PBF, in which force chains in the powder pile are identified as the central mechanism for transmitting forces from the recoater to the powder bed. Experimental data on the corresponding macroscopic recoating forces in sand binder jetting are sparse. Based on this research gap, this work presents an experimental quantification of the tangential and normal recoating forces in sand binder jetting under varied process conditions. Tangential forces parallel to the recoating direction and normal forces perpendicular to the powder bed surface are measured directly with two load cells, allowing the resulting force vector and its direction to be evaluated. The combination of these components characterizes the macroscopic mechanical loading on the powder bed during recoating and complements the particle-scale force chain mechanisms described in the simulation literature with experimental data for sand systems. Specifically, this work examines how blade angles between 70° and 92° influence the tangential and normal recoating forces, how roller circumferential speeds between 0 mm/s and 500 mm/s affect these forces and how the forces change at transitions between unprinted and printed areas. The measurements are carried out on an experimental printing system in which material application is separated from powder bed smoothing, corresponding to commercially available systems and allowing the results to be transferred to many commercial sand binder jetting machines.

2. Experiment bench and measuring device

The investigations in this paper are carried out for the binder jetting process using sand. Sand as material is a differentiating factor compared to the previous investigations in literature. The particles are essentially larger and more irregular in shape than, for example, in metal PBF. The tangential (parallel to the recoating line) and normal (perpendicular to the recoating line) recoating forces are investigated. An experiment rig designed at Fraunhofer IGCV, shown in Fig. 5, is used for the experiments.

The experiment bench is designed based on commercially available sand binder jetting systems and adapted for experimental investigation of the process. It consists of an Isel LES 5 linear drive (isel Germany GmbH, Germany) for each direction. The recoater and print head unit are mounted on the x-axis. The print head is moved in the y-direction via its own linear axis. The build platform for the powder bed and the measuring device for force measurement are mounted on the z-axis. A Starfire SG1024MA (FUJIFILM Dimatix, USA) with 1024 nozzles, a drop size of 80 pl, and a resolution of 400 dpi is used as the print head.

Preliminary experiments show that the amount of sand applied should be kept as constant as possible, as the recoating forces are sensitive to fluctuations in quantity. For this reason, the recoater unit consists of separate application unit (conveyer belt) and smoothing unit (blade or roller recoater), see Fig. 6.

The material application unit in Fig. 6 is based on the conveyor belt principle. A storage container for the sand to be applied is positioned on a conveyor belt at an adjustable distance from the latter. During the movement in the opposite recoating direction, the conveyor belt

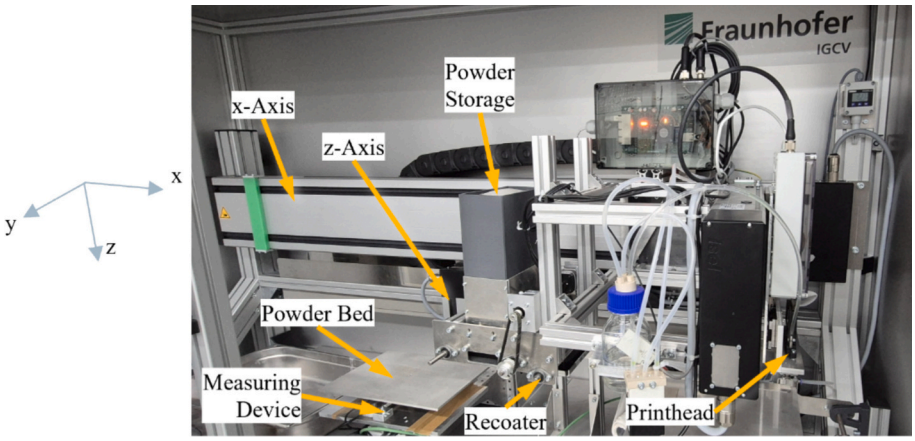

Fig. 5. Experimental bench for investigating recoating forces, developed at Fraunhofer IGCV.

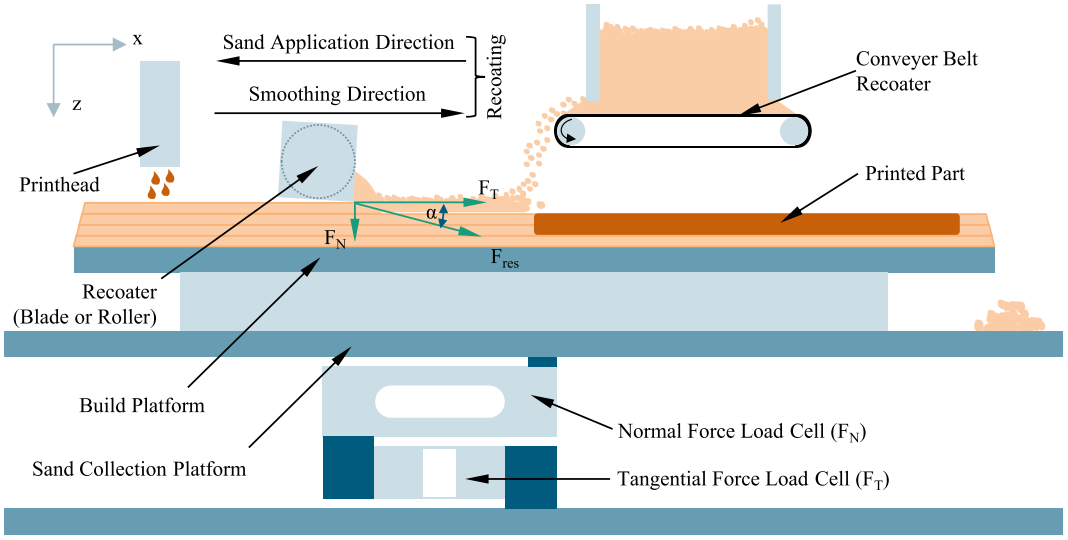

Fig. 6. Experiment apparatus and measurement setup for investigating the recoating forces.

transports the powder onto the powder bed. The amount of powder deposited can be precisely adjusted by changing the distance between the powder container and the conveyor belt or the conveyor belt speed. Despite minor variations in powder delivery, the applied amount of sand plus was determined empirically. The smoothing unit is mounted independently of the depositing device to smooth the powder bed.

The experimental procedure is as follows:

1. The build platform moves down by the layer thickness plus a safety margin of 0.5 mm to ensure complete layer coverage.
2. The x-axis moves across the build platform (in the opposite recoating direction, to the left). At the same time, the conveyor belt begins to apply sand.
3. After completely crossing the build platform, the x-axis and conveyor belt stop.
4. To achieve the exact layer height and a homogeneous, smooth surface, the build platform moves to the correct z-height (layer thickness).
5. The recoater moves back (in the recoating direction, to the right) over the build platform and smooths the layer. Excess sand falls onto the sand collection platform. The sand remains in the weighing balance.
6. For printed areas, the print head then prints the binder into the layer.
7. The process restarts with step 1.

The speeds can be set individually, including the recoating velocity. When printing the build area, on the right-hand side of the build area binder is applied, as shown in Fig. 7. In the control experiment, there is no binder applied on the right-hand side of the build area. Subsequently, the process starts again from the beginning, as described in Fig. 1.

The recoater geometry can be individually modified by the selected setup. The conveyor belt and, if applicable, the recoater roller are each driven by stepper motors and controlled by a Beckhoff soft programmable logic controller (PLC). The measuring device for force measurement consists of a Tedea Huntleigh 2 kg load cell for measuring the normal force and a RS PRO 600 g load cell for measuring the tangential force, which are shown in Fig. 6.

The two load cells are connected in series. With this recoating principle, the sand, which is removed from the powder bed by the action of the recoater, drops onto the sand collection platform at the side of the powder bed. To avoid weighing differences resulting from this procedure, a sand collecting platform is placed at a distance below the build platform to catch the falling sand. With this principle, the sand falling from the powder bed remains on the load cell and does not influence the force measurement. The serial arrangement of the two single-point load cells results in mechanical coupling. Two effects are addressed: Tilting moments and crosstalk between the load cells. To address tilting moments, we use single-point load cells. Forces applied in one direction partially affect the measurement of the other load cell. To quantify and

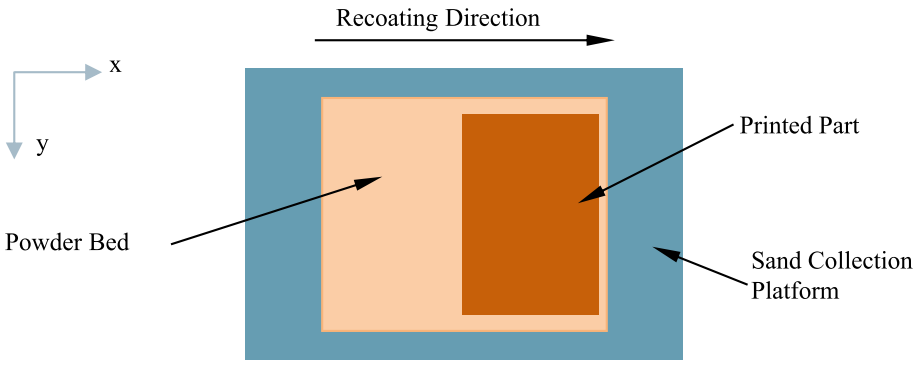

Fig. 7. Powder bed with unprinted and printed areas for investigating the influence of printed areas on the recoating force.

correct this cross-talking effect, calibration experiments were performed:

- Tangential direction: Via a calibrated spring balance known horizontal forces (0–100 mN) were applied
- Normal direction: Calibrated weights (resulting in forces 0–2000 mN) were placed on the build platform

Subsequently linear regressions of the recorded load cell outputs from both calibration experiments yielded the correction factors. Resulting tilting effects contribute to measurement uncertainty but are not expected to systematically bias the results. The evaluation is based on the measured recoating forces. The tangential force F_T corresponds to the corrected horizontal force, and the normal force F_N corresponds to the corrected vertical force. To determine the total recoating force, the magnitude of the forces is calculated, which is described in the evaluation as the force vector F_{res}. The force angle α describes the angle between the tangential force F_T and the force vector F_{res}. These values are highlighted in Fig. 6.

The position and force data of the system is evaluated and recorded at 500 Hz via the soft PLC and TwinCAT. This results in a sample time of 2 ms. A FIR filter is used for noise suppression. Both measurement signals are processed with a Savitzky-Golay filter. The parameters are set as follows in Table 1:

2.1. Recoater geometries

A square blade with a cross-section of 20 mm × 20 mm and a rotating roller with a diameter of 20 mm are examined, as shown in Fig. 8. The blade can move over the powder bed at an adjustable angle, while the roller is driven by a belt drive with variably adjustable speeds in the counterclockwise direction to the recoating direction.

In industrial designed recoaters applying and smoothing of the layer to be built is conducted in one single step. To separate the forces applied by the sand from the recoating forces both the applying and smoothing step are conducted separately in this study. The square blade cross-section was selected to match industrial blade designs. The blade thickness may influence the powder flow at the trailing edge, as the thick blade body partially restricts particle backflow. Thin blades are used in metal PBF. However, with sand particles the relative blade-to-particle size ratio is smaller than in metal PBF, potentially reducing this effect. Comparative studies with different blade thicknesses are beyond the scope of this work.

Table 1
Parameters of the Savitzky-Golay filter.

Parameter	Value
Window Length	85
Polynomial Degree	4

The experiment parameters for the two geometries are listed in Table 2.

The angle of the square blade refers to the angle between the powder bed and the blade in the recoating direction at the front. The circumferential speed of the rotating roller is specified in the counterclockwise direction.

2.2. Experimental plan

The tangential and normal recoating forces that influence the shear behavior of the powder bed in front of the recoater are to be investigated. The parameters recoating velocity, blade angle, roller circumferential speed and layer thickness are included for this purpose. For a better evaluation of the relative speed in the recoater area, the roller circumferential speeds are examined instead of the roller speed. The parameters to be investigated are listed in Table 3. To isolate the effect of printed layers on recoating forces, control experiments without binder application were conducted. In these control experiments, the identical measurement protocol was followed but no binder was applied. Hence the control experiments are marked with “N” in the table. The comparison between experiments with and without binder respectively printed layers allows distinguishing force effects caused by printed layers from those caused by other factors. The standard parameters used in this investigation for the blade and roller are shown in bold. In the preliminary experiments, it was found that the results can only be compared to each other within a narrow time frame. Indeed, environmental factors and empirical uncertainties such as air humidity or sand moisture have a strong influence. The experiments marked “N.A.” in Table 3 could therefore not be included in the evaluation of the results.

For better evaluation of the relative speed in the recoater area, the roller circumferential speed is reported instead of the angular velocity. This allows direct comparison with the recoating velocity and enables calculation of the relative speed between the roller surface and the powder bed. At a circumferential speed equal to the recoating velocity, the relative speed at the contact point is zero. Higher circumferential speeds result in the roller surface moving faster than the recoating motion.

To assess the dispersion of the results, each experiment is carried out three times. Preliminary experiments showed that the surface quality of the build platform has a significant effect on the experiment results and that this influence becomes negligible from layer 4 onwards. Therefore, only layers 4–10 of an experiment are evaluated below. Since the first layer cannot be printed in experiments due to the build platform, a base layer (layer 0) is used in each experiment. The layer configuration with printed layers is shown in Fig. 9. This results in a total of 21 evaluable layers per data point from the three experiments and the seven evaluated layers.

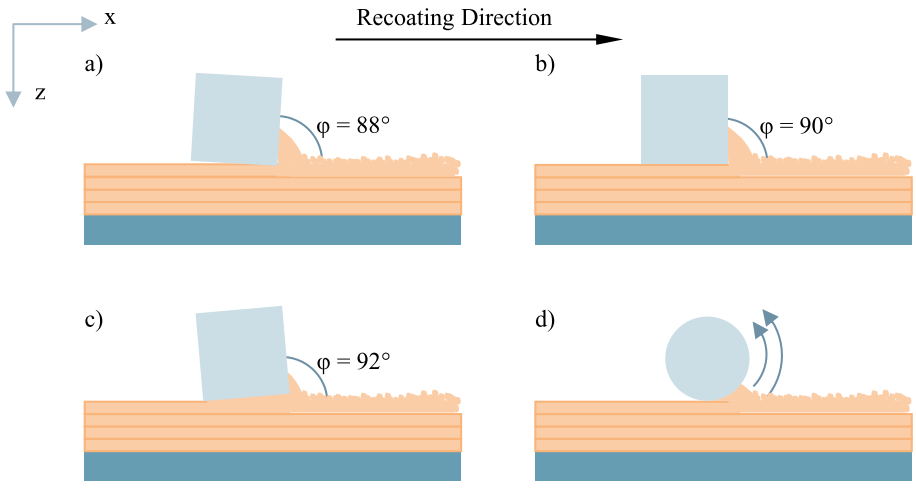

Fig. 8. Illustration of the recoater geometries investigated.

Table 2
Recoater geometries and parameters investigated.

Geometry	Parameters investigated
Square blade	70°, 75°, 80°, 85°, 88°, 90°, 92°
Rotating roller	0 mm/s, 100 mm/s, 300 mm/s, 500 mm/s

2.3. Sand, binder and additives

The sand used in this study for the experiments is GS14RP, a commercially available silica quartz sand for rapid prototyping in foundry from Strobel (Strobel Quarzsand GmbH, Germany). The average sand grain diameter is D_{50} = 135 µm, the cumulative distribution according to the manufacturer is shown in Fig. 10. The characteristic values are: D_{10} = 94 µm and D_{90} = 174 µm. The AFS number is 95.

To complement the particle size distribution, the morphology of the sand grains was examined by SEM. Fig. 11 shows representative electron microscopy images of GS14RP particles. The grains exhibit an irregular shape with rough surfaces and a moderate degree of sphericity. According to the manufacturer, the uniformity ratio is 90%. These characteristics distinguish it from the spherical morphology of typical metal AM powders.

In the experiments with printed layers, binder is selectively printed by the print head. The binder used is the inorganic binder Cordis AM101 (Hüttenes Albertus, Germany) based on a modified sodium silicate solution. The target binder-to-sand ratio is 3.5 wt% in the actual experiments, which corresponds to a volumetric saturation of 10.6% of the porous volume.

Interlayer curing is known to cause deformations of the printed parts. Nonetheless, to address the binder drying the time between binder deposition and the subsequent recoating step was held constant in all the

Table 3
Examined parameter combinations. The standard configurations are shown in bold.

Recoating speed	Blade/roller	Layer thickness	Binder	Recoating speed	Blade/roller	Layer thickness	Binder
100 mm/s	70°	280 µm	Y/N				
100 mm/s	75°	280 µm	Y/N				
100 mm/s	80°	280 µm	Y/N	300 mm/s	80°	280 µm	Y/N
100 mm/s	85°	280 µm	Y/N	300 mm/s	85°	280 µm	Y/N.A.
100 mm/s	**88°**	**280 µm**	Y/N	300 mm/s	88°	280 µm	Y/N
100 mm/s	90°	280 µm	Y/N	300 mm/s	90°	280 µm	Y/N.A.
100 mm/s	92°	280 µm	Y/N				
100 mm/s	0 mm/s	280 µm	Y/N	300 mm/s	0 mm/s	280 µm	Y/N
100 mm/s	50 mm/s	280 µm	Y/N				
100 mm/s	**100 mm/s**	**280 µm**	Y/N	300 mm/s	100 mm/s	280 µm	Y/N
100 mm/s	200 mm/s	280 µm	Y/N				
100 mm/s	300 mm/s	280 µm	Y/N	300 mm/s	300 mm/s	280 µm	Y/N
100 mm/s	400 mm/s	280 µm	Y/N				
100 mm/s	500 mm/s	280 µm	Y/N	300 mm/s	500 mm/s	280 µm	Y/N

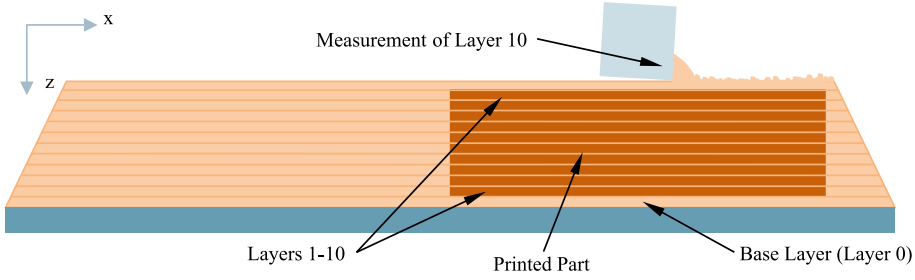

Fig. 9. Recoating force measurement, here as an example for layer 10.

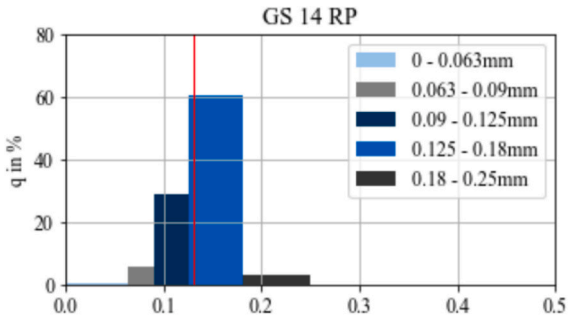

Fig. 10. Grain size distribution of GS14RP sand used in this work.

experiments via the process design and was 8 s. The binder state during recoating therefore corresponds to an early point along the natural drying trajectory of the binder itself.

Sands are mixed with additives to improve their mechanical properties and facilitate handling after the printing process. To ensure comparability between the experiments with and without printed layers, all sand batches were prepared identically with the additives listed in Table 4 before use. Without these additives, the control experiments ("no binder") would have different powder flow properties, affecting the comparison.

The additives AM401 and AM50 improve component properties such as edge sharpness and flowability of the sand. The additive from VoxelJet (VoxelJet AG, Germany) is a cold-curing hardener based on waterglass ester. The residual moisture content of the material was measured at 0.32% by a Kern Moisture Analyzer DBS60–3. The bulk and tapped densities were measured to a bulk density of 1.411 g/cm^3 and a tapped density of 1.639 g/cm^3, resulting in a Hausner ratio of 1.162.

2.4. Data processing and evaluation

The single experiments are evaluated layer by layer. For these layers, the normal and tangential force data are evaluated and analyzed in specific regions. An example of a recorded measurement for a layer with a printed part is shown in Fig. 12.

The measurement record describes the tangential force (blue) and normal force (brown) curves in mN vs. the x-axis position, with the recoating direction from left to right. The build platform area is located between the black-lined vertical lines. The purple vertical line marks the beginning of the printed area.

Both forces are set to zero via the moving average in front of the build platform in order to evaluate the data for the current layer. The evaluation algorithm detects the start and end of the layer by determining the local maximum of the force change. This is necessary due to the layer-by-layer change in the powder bed edge as a result of the angle of repose of sand. For further data processing, regressions are calculated for each area and force. These are created for the unprinted area (yellow/pink) and the printed area (green/gray).

The force curves jump at the start of the build platform when the recoater hits the sand. The force curves rise due to the growing powder pile in front of the recoater, with tangential and normal force curves having different slopes. During recoating, the excess sand falls onto the sand collecting platform at the edges of the build platform. In the measurement balance of the normal force curve, the falling sand is retained by the selected design. At the transition to printed surfaces, there is a sharp increase in the force in both curves. The slope of the force curves may change over the printed surfaces.

The following diagrams always evaluate the mean value of the two regression curves over the printed area, which are marked with an "X" in Fig. 12. The portion of the recoater interacting with the powder bed is defined as contact length. As there is no box in the experimental setup, the contact length depends on the powder bed geometry, which undergoes a change with each layer due to the angle of repose at the bed

Table 4
Sand binder system used.

Additive	Form	Amount in wt%-sand
Cordis AM401	Powder	1%
Cordis AM50	Liquid	0,02%
VoxelJet IOB Additive C	Liquid	0,25%

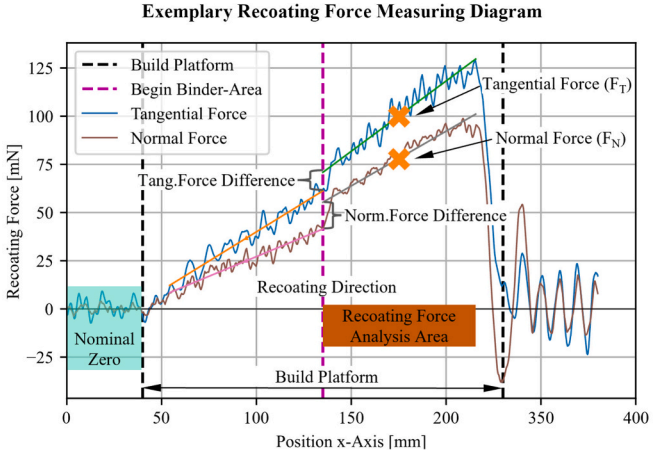

Fig. 12. Example measurement data diagram with marked evaluation areas.

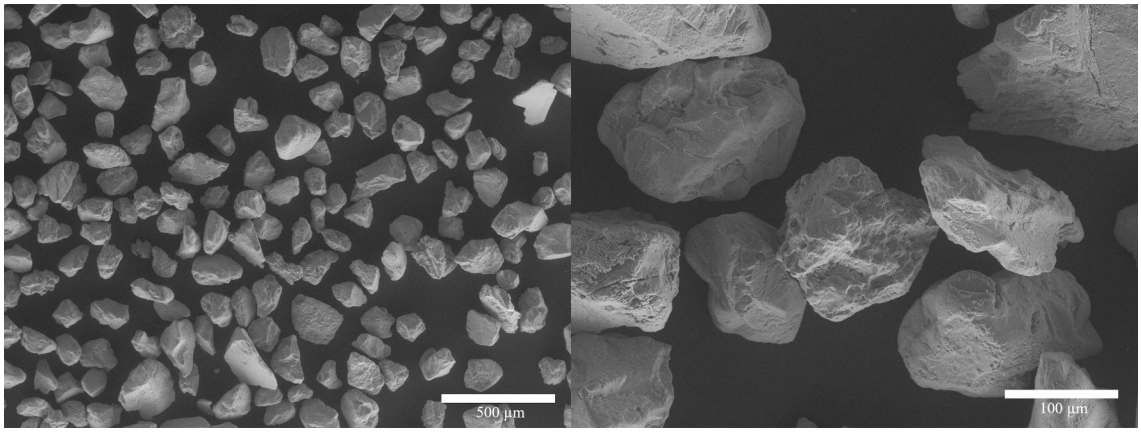

Fig. 11. Electron microscopy image of the GS14RP sand used in this study.

edges. Forces are normalized per centimeter of recoater contact length to enable comparison across layers. For the used sand-binder system experiments showed an angle of repose of 33.5°. The contact length increases linearly from layer 1 to layer 10 as the tapered edges extend. For the evaluated layers 4–10 as mentioned in Section 2.2, layer 7 represents the median contact length of 15.37 cm for the layer thickness of 280 µm, 15.05 cm for the layer thickness of 420 µm and 14.74 cm for the layer thickness of 560 µm.

The experiment results are presented below for each individual parameter. The recoater geometry and velocity results are shown in Section 3.1 evaluating neutral to inclined angles. Section 3.2 discusses the results for the force difference at the beginning of a printed part, respectively the transition from unprinted to printed areas, as a central experiment to measure the part sensitivity for illustrating the conditions during an eventually layer displacement.

3. Results

3.1. Recoating forces

The influence of recoater geometry on the recoating forces is examined below.

3.1.1. 100 mm/s recoating velocity

For this purpose, the measurement results shown in Fig. 13 are considered at a layer thickness of 280 µm and a recoating velocity of 100 mm/s.

The Fig. 13a and b show the tangential force (F_T) and normal force (F_N) above the recoater geometry. To estimate the total recoating force acting, Fig. 13c shows the magnitude of the tangential and normal forces above the recoater geometry. Fig. 13d shows the resulting force angle above the recoater geometry. This order of presentation is maintained for the following experiments. The mentioned values are the median values of the data points.

The tangential and normal forces for different blade angles show that both decrease as the blade angle increases. In the range examined, they approach at 90° values of 4.9 mN/cm (tangential force) and 1.8 mN/cm (normal force). The maxima at a blade angle of 70° over printed areas are 7.7 mN/cm (tangential force) and 6.5 mN/cm (normal force). As the blade angles become more inclined, there are greater differences between printed layers and control experiments. The forces over printed areas are higher than over unprinted areas. At a blade angle of 85°, the tangential force shows a local minimum of 4.3 mN/cm. However, the normal force does not exhibit a corresponding minimum at this angle.

A similar trend is observed for the force magnitude. As the blade angle increases, the values at 90° approach a force of 5.3 mN/cm. Moreover, at steep blade angles (70° - 80°), the forces over printed areas are significantly higher at 10 mN/cm than over unprinted areas with values of flat 7.4 mN/cm. The maximum is 10.0 mN/cm at a blade angle of 70° over printed areas. In contrast, the force is higher at a blade angle of 88° over unprinted areas than over printed areas.

The force angle decreases in the examined range between 40.1° and 20.5°, with sharper blade angles exhibiting higher force angles. It follows that the normal force changes more significantly than the tangential force in the examined range.

In the following Fig. 14, the influence of the roller circumferential speeds on the recoating forces at a recoating velocity of 100 mm/s is considered analogously.

The evaluation of the tangential and normal forces shows a non-linear decrease in forces with increasing roller circumferential speed. The forces drop from 13.6 mN/cm (tangential force) and 17.6 mN/cm (normal force) to 4.0 mN/cm (tangential and normal force), a value at

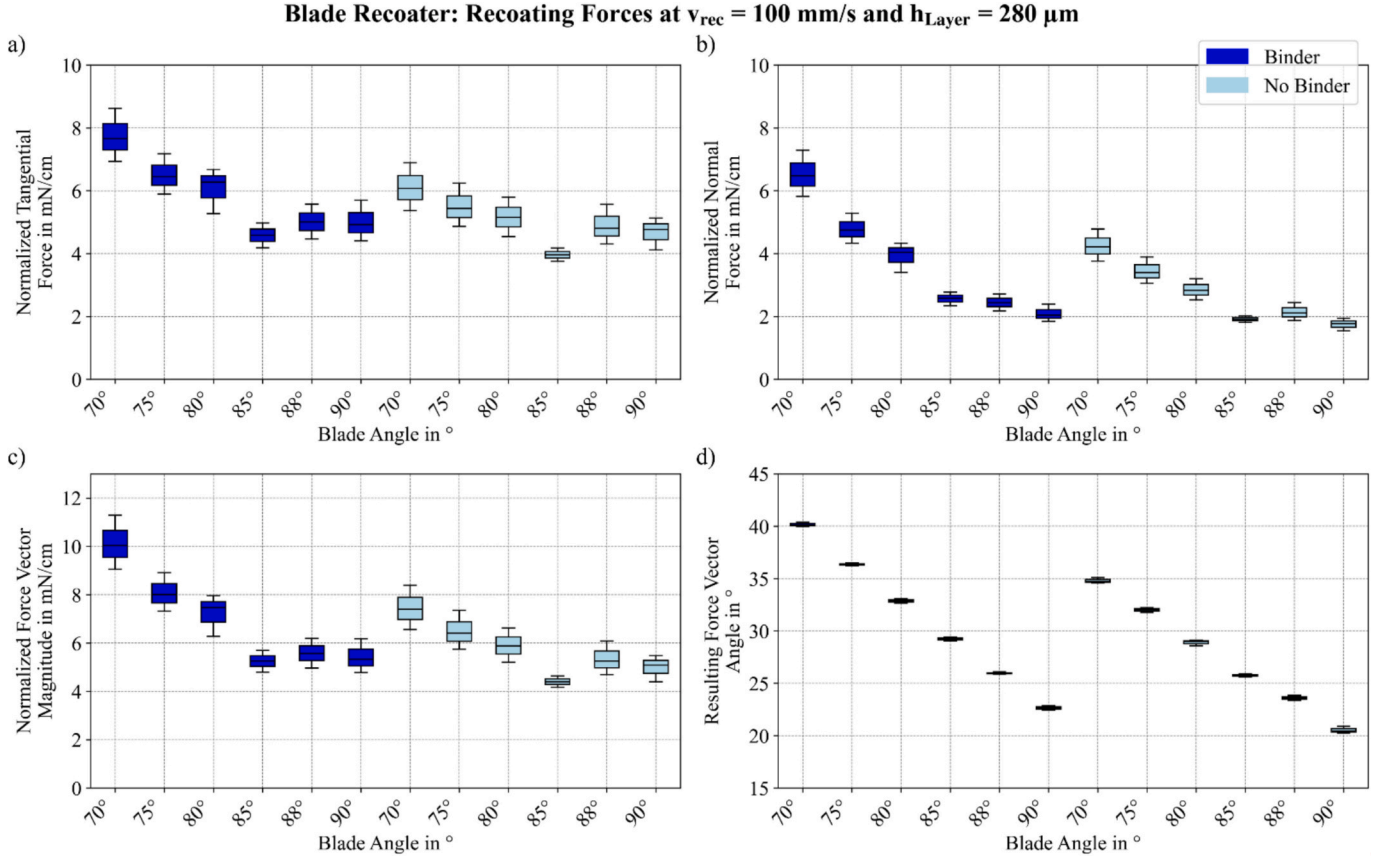

Fig. 13. Recoating forces of printed parts and control experiments per centimeter recoater at different blade angles: a) normalized tangential force, b) normalized normal force, c) resulting normalized force vector magnitude, and d) resulting force vector angle.

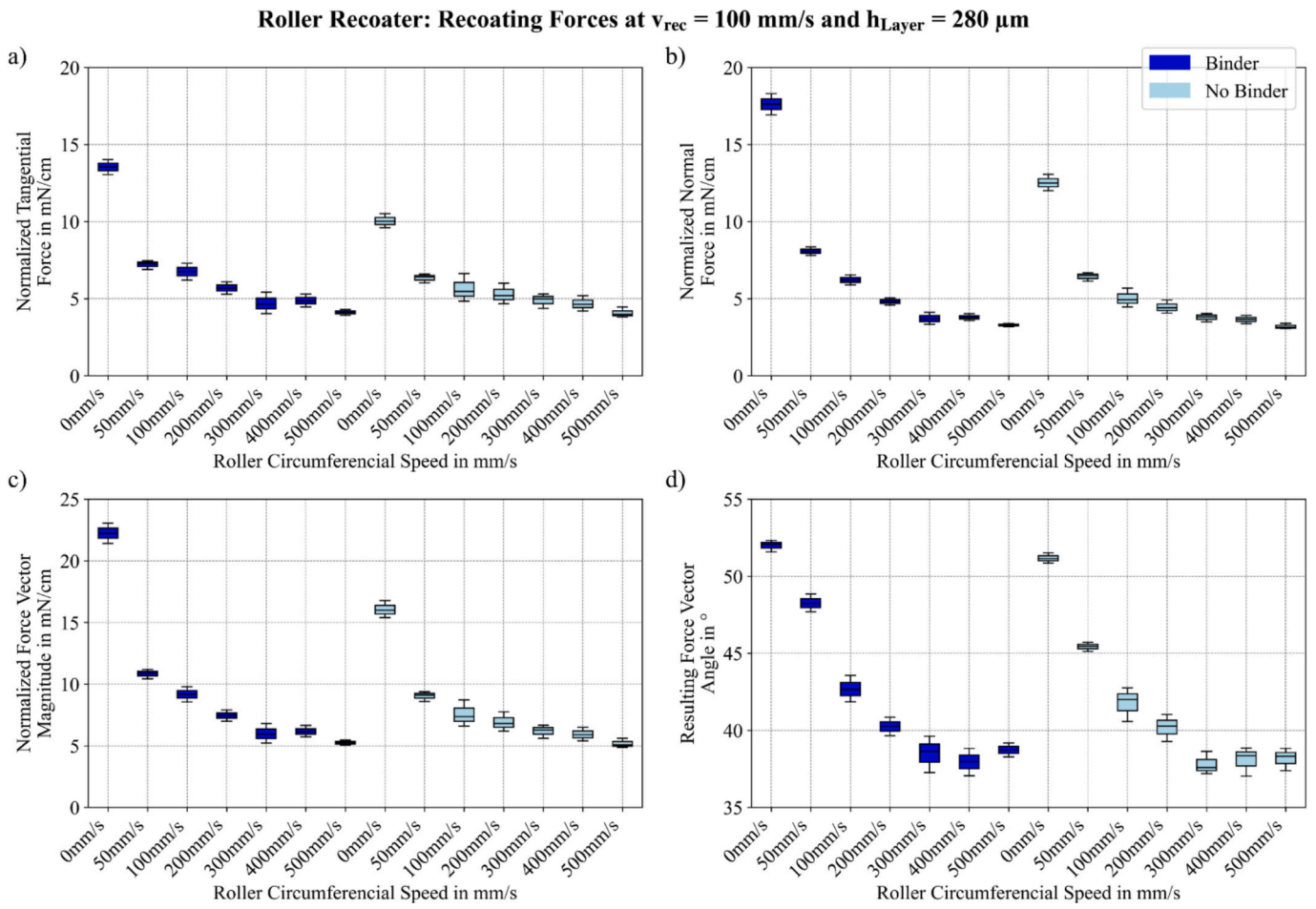

Fig. 14. Recoating forces of printed parts and control experiments per centimeter recoater at the roller circumferential speeds investigated: a) normalized tangential force, b) normalized normal force, c) resulting normalized force vector magnitude, d) resulting force vector angle.

which a stabilization occurs. This trend can also be seen in the evaluation of the force magnitude. The values are higher over printed areas than over unprinted areas. At high speeds, the values hardly change. The force angle only changes significantly in the range up to 100 mm/s and fluctuates around 38.3° at higher circumferential speeds. Force angles in the range around 45.0° show that the tangential and normal forces have a similar magnitude.

The results for the blade and roller show that, apart from a roller circumferential speed of 0 mm/s, the tangential forces are in similar ranges. The roller has higher normal forces than the blade. The force magnitude is comparable for both geometries. A comparison of the force angles shows that the resulting force vector is oriented more horizontally, i.e. smaller angle relative to the powder bed surface) for blades than for rollers.

3.1.2. 92° blade angle

Blade angles above 90° seem to represent a critical operating regime. Due to significantly exceeding recoating forces, the results observed at a blade angle of 92° are presented separately to preserve the clarity of trends observed at the blade angle range from 70° to 90°.

Fig. 15 shows the results for all blade angles examined. The results reveal significantly higher values for both the tangential force at 40.5 mN/cm and the normal force at 79.7 mN/cm than for the other blade angles. This difference is greater for the normal force. At 89.4 mN/cm, the force is also higher than the value for the other blade angles. Evaluating the force angle shows that, at 63.0°, it is higher than the values for the other blade angles and is clearly influenced by the normal force. This effect differs from the other blade angles examined. Overall, all values examined for a 92° blade angle are higher than the other results in this paper.

The force differences at the transition from unprinted to printed areas are also examined for a blade angle of 92°. The results are shown in Fig. 16.

Fig. 16a and b show the force difference at the transition from unprinted to printed areas with a blade angle of 92°. At 97.4 mN/cm, the tangential force difference is significantly higher than for the other blade angles investigated. The same applies to the normal force difference, which has a value of 203.9 mN/cm.

A comparison with the roller geometry shows that the clamping and compression effect is greater at a blade angle of 92° than for the roller geometry.

3.1.3. 300 mm/s recoating velocity

The results for a recoating velocity of 300 mm/s are shown below in Fig. 17. The presentation is the same as in the results for a recoating velocity of 100 mm/s.

The experiment results on the influence of recoater geometry at a recoating velocity of 300 mm/s and a layer thickness of 280 µm are shown in Fig. 17. The tangential forces in the investigated range are between 3.0 mN/cm and 4.1 mN/cm and remain approximately constant. The normal forces are in the high range at 2.6 mN/cm and decrease with increasing blade angle to 1.1 mN/cm at a 90° blade angle. The force fluctuates between 3.2 mN/cm and 4.9 mN/cm. When comparing the experiments with and without printed areas, the forces over printed areas are always higher than over unprinted areas. The force angle decreases with increasing blade angle from 32.8° at an 80°

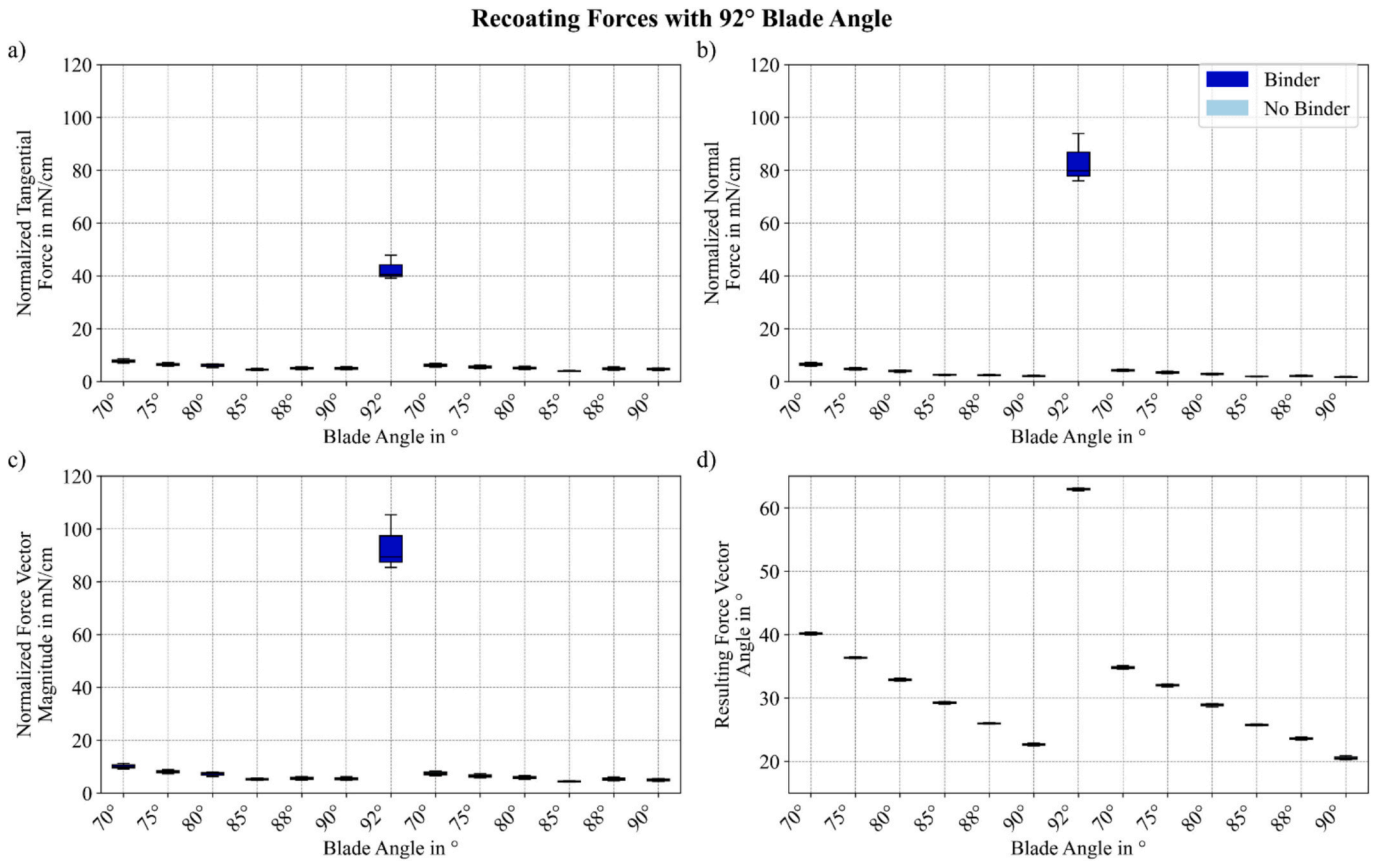

Fig. 15. Investigation of the recoating force of printed parts and control experiments per centimeter at a blade angle of 92° in comparison to other blade angles: a) normalized tangential force, b) normalized normal force, c) normalized force vector magnitude, and d) resulting force vector angle.

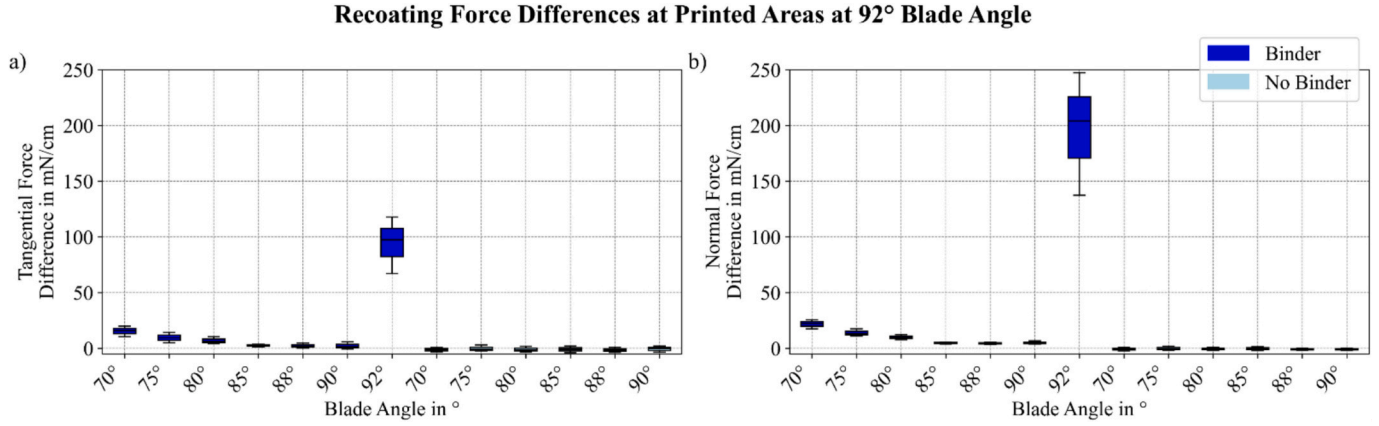

Fig. 16. Investigation of the binder transition at a blade angle of 92° in comparison to other blade angles.

blade angle to 19.3° at a 90° blade angle over the printed area. It follows that the normal force changes more with increasing blade angle than the tangential force.

Fig. 18 shows the evaluation of the experiments with roller geometry at a recoating velocity of 300 mm/s.

The evaluation of the tangential and normal forces shows that the recoating forces decrease with increasing roller circumferential speed. They stabilize at 6.1 mN/cm. The maxima are always at 0 mm/s roller circumferential speed. The maximum tangential force is 12.8 mN/cm, and the maximum normal force is 17.2 mN/cm. The forces are higher over printed areas than over unprinted areas at the same roll circumferential speed.

The force magnitude has a similar curve to the tangential and normal forces. The maximum is 21.4 mN/cm. The values decrease non-linearly and settle at 8.0 mN/cm as the roller circumferential speed increases. For the force magnitude, the values are higher over printed areas than over unprinted areas at the same roller circumferential speed.

The force angle is around 50°. This observation indicates a uniform change in the proportions of tangential and normal force at different roller circumferential speeds. Again, the values are higher over printed areas than over unprinted areas.

For all blade geometries examined, both the tangential and normal forces are lower than for all roller circumferential speeds examined. The force angle decreases from 32.8° at a blade angle of 80° to 19.3° at a

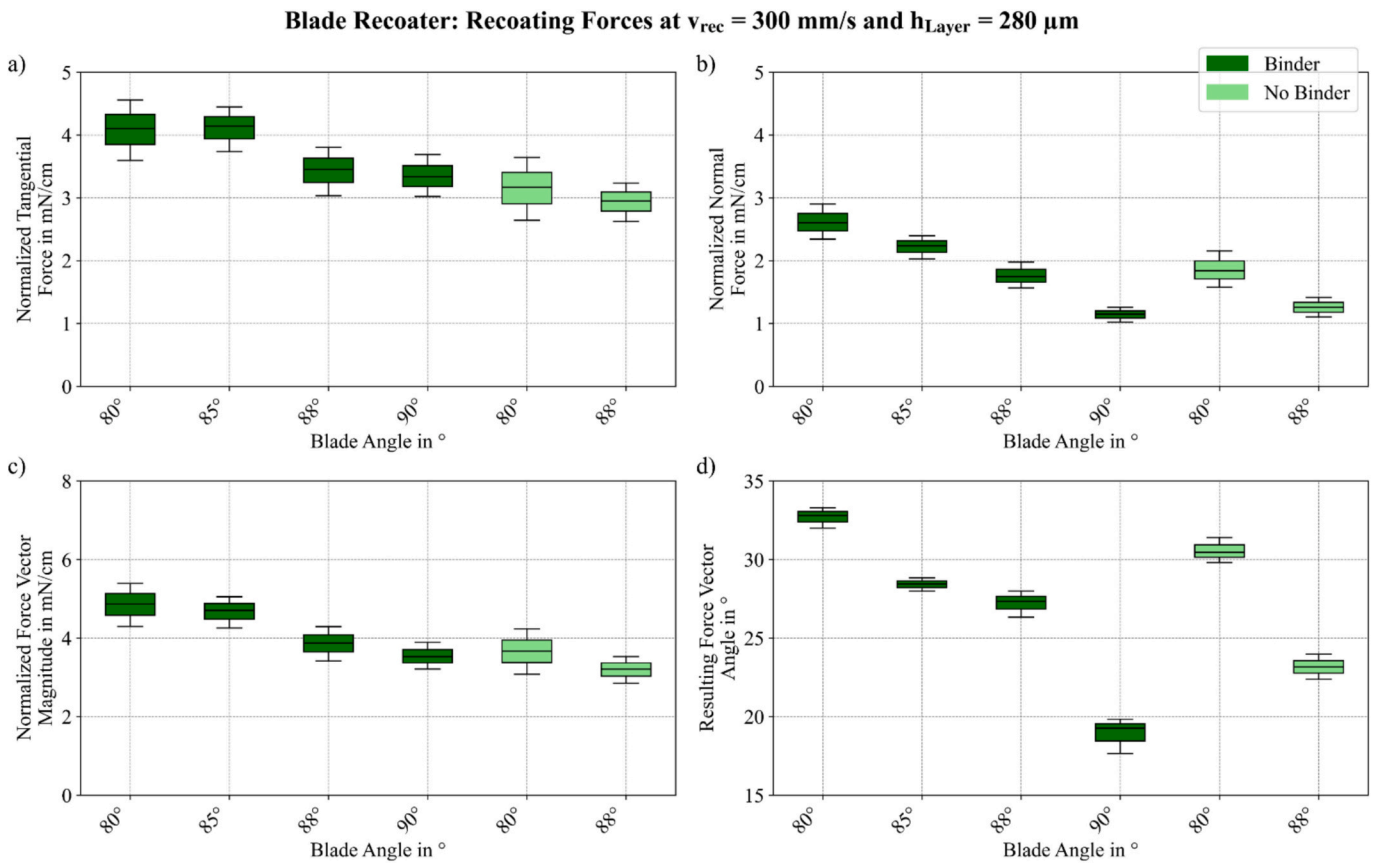

Fig. 17. Recoating forces of printed parts and control experiments at different blade angles. a) normalized tangential force, b) normalized normal force, c) normalized force vector magnitude, and d) resulting force vector angle.

blade angle of 90°, thus becoming flatter. The force angles for the roller circumferential speeds examined are 50.0°, which is steeper than those for the blade angles examined.

To describe the influence of recoating velocity on recoating forces, we evaluate the recoating velocity of 100 mm/s and 300 mm/s at the layer thickness of 280 µm. For the blade recoater we consider the blade angle of 88° and for the roller recoater the roller circumferential speed of 100 mm/s. The results from Figs. 13 and 17 respectively Figs. 14 and 18 are observed.

With the blade recoater, the recoating forces decrease as the recoating velocity increases. This difference is greater for the tangential force than for the normal force. The tangential force decreases from 5.0 mN/cm to 3.5 mN/cm over printed areas and from 4.8 mN/cm to 3.0 mN/cm on unprinted areas. The normal force decreases from 2.4 mN/cm to 1.7 mN/cm and from 2.1 mN/cm to 1.3 mN/cm, respectively. Likewise, the recoating force magnitude is reduced. The force angle increases over printed areas and decreases over unprinted areas as the recoating velocity increases. Over printed areas, the force therefore acts deeper into the powder bed.

For the roller recoater, the tangential and normal forces over printed areas consistently show higher force values compared to unprinted areas. The tangential force shows no speed-dependent differences over unprinted areas, but there is an increase over printed areas. The normal force shows slightly higher forces over unprinted areas at higher recoating velocity. Over printed areas, the normal force is significantly higher at 12.0 mN/cm at a recoating velocity of 300 mm/s than at 6.2 mN/cm at a recoating velocity of 100 mm/s. This behavior is also reflected in the force magnitude. The force angles are 42.3° at a recoating velocity of 100 mm/s and 51.6° at a recoating velocity of 300 mm/s. As a consequence, the main resulting direction of the recoating force changes deeper into the powder bed as the recoating velocity raises.

The results show that the effect of the recoating velocity on the forces is lower for the blade recoater than for the roller one. The forces decrease with higher recoating velocity. Especially over printed areas, the force is significantly higher for rollers than for blades. While the recoating force acts mainly tangentially with blades, the direction of action changes from tangential to steep downward with increasing recoating velocity for rollers.

No results could be evaluated for a blade angle of 92° at 300 mm/s.

3.2. *Force differences at part boundaries*

The literature describes impacts that occur at the transitions from unprinted to printed areas [13,17]. To isolate the effect of printed areas on recoating forces, control experiments without binder application were conducted. In the control experiments, marked with “no binder”, the same measurement protocol was followed, but no binder was applied. The comparison between experiments with binder, marked with “binder”, and without binder distinguishes force differences caused by printed layers from that cause by other factors.

To investigate this part sensitivity, the partial regression lines from Fig. 12 are examined. More specifically, the difference in regression force at the end of the first (unprinted) section and at the beginning of the second (printed) section is considered (green-orange and gray-pink regression lines, respectively). This corresponds to the force difference at the purple line in Fig. 12. This location has a part edge that is comparable to those in literature. The recoater geometry and velocity are considered.

The following section examines the force differences at the transition from unprinted to printed areas depending on the recoater geometry. Fig. 19 shows the results for a layer thickness of 280 µm and recoating velocity of 100 mm/s and 300 mm/s for different blade angles.

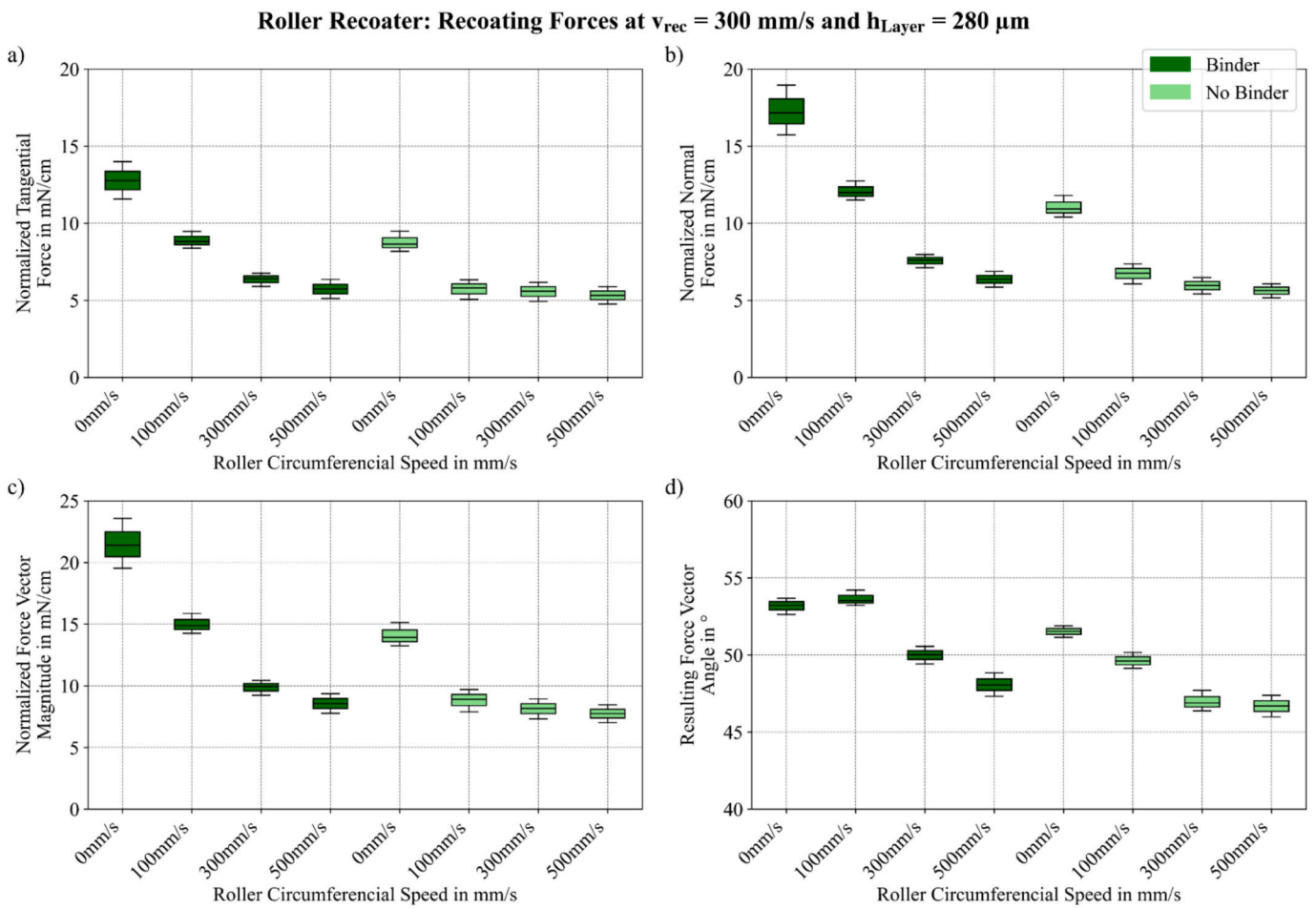

Fig. 18. Recoating forces of printed parts and control experiments at different roller circumferential speeds. a) normalized tangential force, b) normalized normal force, c) resulting normalized force vector magnitude, and d) resulting force vector angle.

At a recoating velocity of 100 mm/s, the tangential and normal force differences before and after the part for varying blade angles show that at a blade angle of 70° the force differences are higher than at a blade angle of 90°. At a recoating velocity of 300 mm/s, the tangential and normal force differences show relatively small variation across blade angle investigated. The tangential force difference ranges from 12.2 mN/cm at 80° to 18.1 mN/cm at 90°. The normal force differences in the investigated range are 5.0 mN/cm and thus tend to be lower than the tangential force differences.

The Fig. 20 shows the results for different roller circumferential speeds.

For the roller circumferential speeds investigated, the tangential and normal force differences decrease with increasing roller circumferential speeds from 42.6 mN/cm and 70.4 mN/cm at 0 mm/s to almost 0.0 mN/cm at 100 mm/s roller circumferential speed. The normal force difference tends to be higher than the tangential force difference in the range investigated. At a recoating velocity of 300 mm/s, the force differences are higher than at a recoating velocity of 100 mm/s and only decrease at higher roller circumferential speeds. Furthermore, they don't approach 0.0 mN/cm but remain elevated.

The control experiments without printed areas show no significant differences in force for blade angles. At different roller circumferential speeds, there are negative differences in the investigated range at low roller circumferential speeds, both in terms of tangential and normal force differences. This results from the regression line generation. While the powder pile increases more at the beginning of the build platform, the forces rise more there. With dividing the regression line into two parts, with less increase at the end of the platform there is a negative difference at the transition from the unprinted to printed area.

As in the previous section we evaluate the recoating forces at 100 mm/s and 300 mm/s recoating velocity to describe the influence of latter on the recoating force differences at the transition from unprinted to printed areas. Again, the results for a layer thickness of 280 µm and a blade angle of 88° respectively a roller circumferential speed of 100 mm/s for recoating velocity of 100 mm/s and 300 mm/s.

The results for the blade recoater have higher force differences at the transition to printed areas at higher recoating velocity. The tangential force difference increases from 2.0 mN/cm at a recoating velocity of 100 mm/s to 12.5 mN/cm at a recoating velocity of 300 mm/s, while the normal force difference increases from 4.7 mN/cm at a recoating velocity of 100 mm/s to 7.7 mN/cm at a recoating velocity of 300 mm/s. A comparison with the results without printed areas shows that these also increase with increasing recoating velocity. The effect is therefore negligible.

The results for the roller recoater show significantly higher force differences at higher recoating velocity. The tangential force difference increases from 3.9 mN/cm at a recoating velocity of 100 mm/s to 42 mN/cm at a recoating velocity of 300 mm/s, while the normal force difference increases from 8.5 mN/cm at a recoating velocity of 100 mm/s to 67.5 mN/cm at a recoating velocity of 300 mm/s. The tangential and normal force differences in the comparative experiment without printed areas are close to 0.0 mN/cm. We thus observe the significant influence of the effect of printed areas.

A comparison of the force differences at the transition to printed areas shows that the roller has a significantly greater effect than the blade. The recoating velocity in particular has a strong influence on the

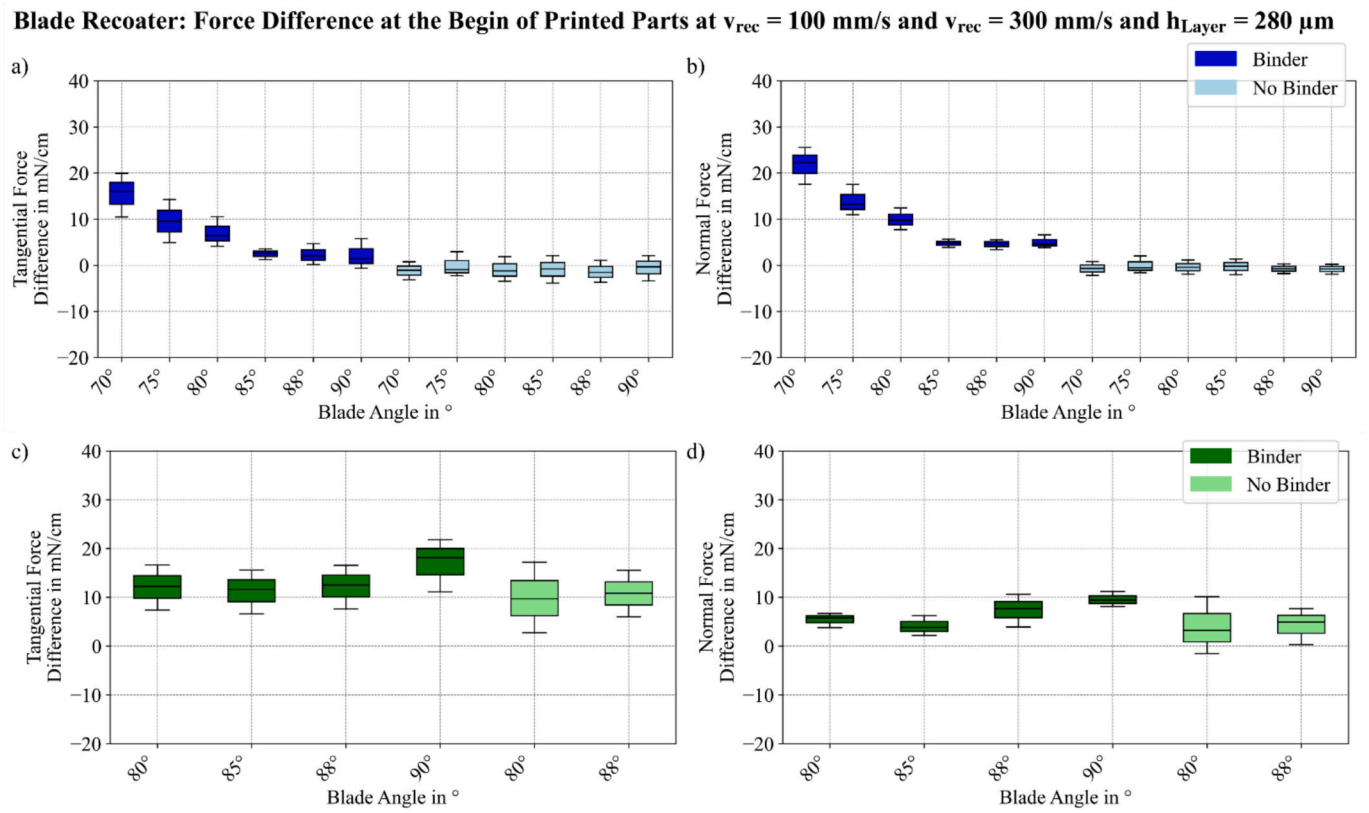

Fig. 19. Force differences at the begin of printed parts and control experiments at different blade angles and recoating velocity: a) normalized tangential force at 100 mm/s recoating velocity, b) normalized normal force at 100 mm/s recoating velocity, c) normalized tangential force at 300 mm/s recoating velocity, d) normalized normal force at 300 mm/s recoating velocity.

values.

4. Discussion

This study measures recoating forces in sand binder jetting in a parameter study. According to the state of the art, these forces can be assigned to the force arcs between the sand particles, whose net force leads to the result in the recoating force. The experimental results are discussed below.

4.1. Influence of recoater geometry on recoating forces

The measurements show that blade angles of 88°–90° yield the lowest recoating forces, with a normalized tangential force of 4.9 mN/cm and a normalized normal force of 1.8 mN/cm at a blade angle of 90°. Forces increase with decreasing blade angle toward 70°. At a blade angle of 70°, the tangential force rises to 7.7 mN/cm and the normal force to 6.5 mN/cm. The force vector angle shows a linear relationship with the blade angle in the range of 70° - 90°, with a “base angle” of approximately 20° at 90°. This means that at steep blade angles, the tangential force dominates, while the normal force gains influence at inclined angles.

This implies that more inclined blades (e.g. 70°) compress the powder bed more strongly, increasing the risk of displacing previously printed layers. The 88° standard angle used in practice represents a good compromise. It minimizes forces while accounting for manufacturing tolerances and avoiding the critical range beyond 90°. Beyond 90°, particles become trapped in the gap between blade and powder bed leading to sharply increased forces. The measured forces at 92° confirm this critical transition.

Because of the unusually high recoating forces measured for the 92° configuration, the powder bed surface was additionally documented after recoating to check whether the elevated forces had a visible effect on the powder bed. Fig. 21 compares the reference layer with the printed part before recoating (Fig. 21a) with the powder bed surface after recoating at blade angles of 88° and 92°.

At 88°, the printed region remains in its intended position after recoating, consistent with the low forces measured for this configuration. At 92°, a clear displacement of the printed region in the recoating direction is visible, corresponding to the substantially higher tangential and normal forces measured under this condition. While these are individual observations rather than systematic image series, they provide a direct visual reference for the mechanical consequence of the elevated forces measured by the load cell measurements.

These findings are consistent with Zhang et al. [14], who reported that tangential forces predominate in blade recoaters. The observation that the recoating force depends mainly on the powder pile size in the recoating direction confirms the DEM predictions of Wang et al. and Chen et al. [6,10], who showed that force chains form primarily in the powder pile in front of the recoater. The smooth blade surface facilitates particle flow from the bottom to the top of the powder pile, as described by Wang et al. [9].

Regarding the transferability to metal AM, the larger sand particles with mean diameter of 140 µm compared to typical metal powder with 40 µm and their irregular grain shape are expected to form more stable force chains. However, the fundamental mechanism of steeper blade angles reducing forces by minimizing the compression zone should apply to both material systems, as it is governed by geometry rather than particle-scale cohesion.

Without circumferential speed (0 mm/s), rollers behave like blades beyond 90°, with high forces due to particle trapping. With increasing circumferential speed, forces decrease non-linearly: from 13.6 mN/cm at 0 mm/s to 4.0 mN/cm at 500 mm/s circumferential speed. Above 200 mm/s forces stabilize at a constant level, defining a basic force angle of

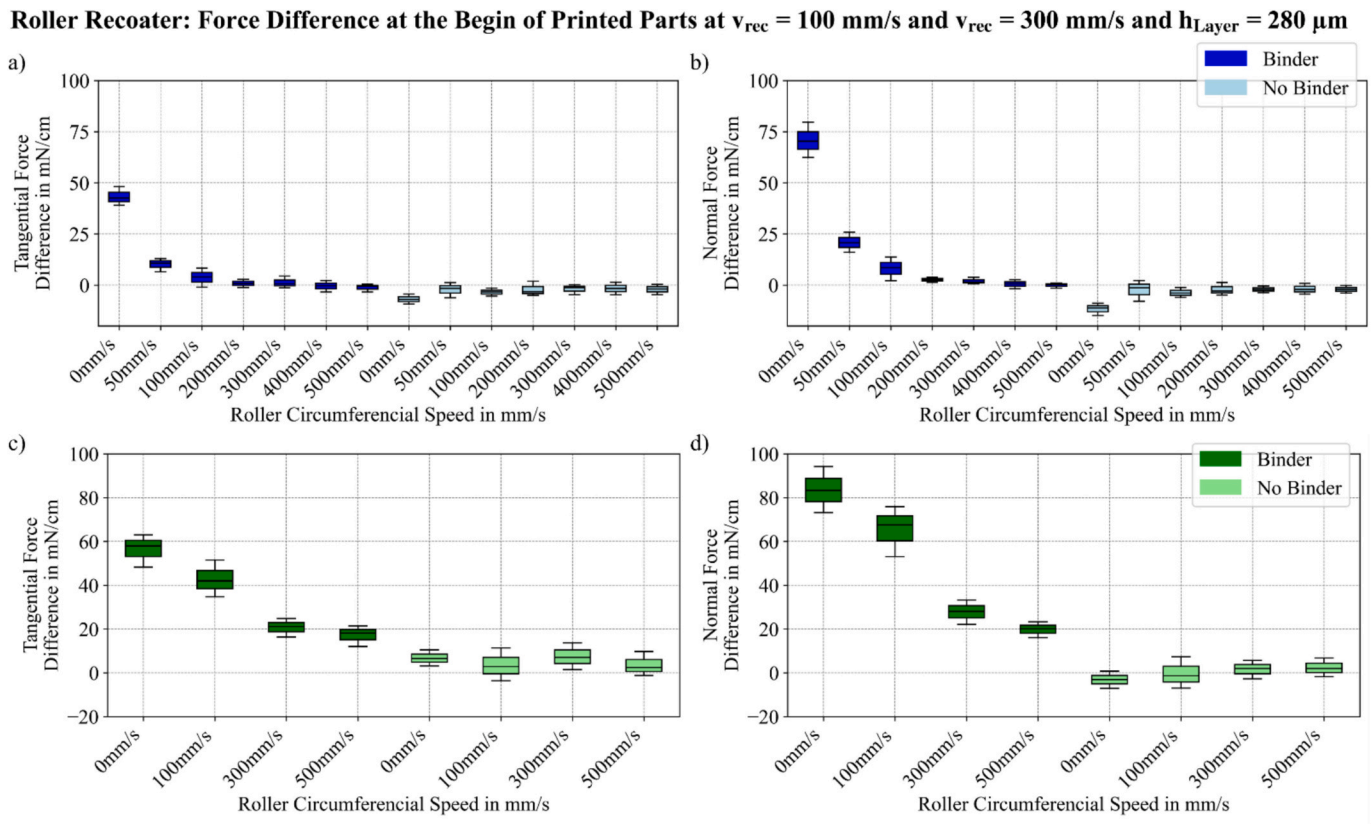

Fig. 20. Force differences at the begin of printed parts ("binder") and control experiments ("no binder") at different roller circumferential speeds and recoating velocity: a) normalized tangential force at 100 mm/s recoating velocity, b) normalized normal force at 100 mm/s recoating velocity, c) normalized tangential force at 300 mm/s recoating velocity, d) normalized normal force at 300 mm/s recoating velocity.

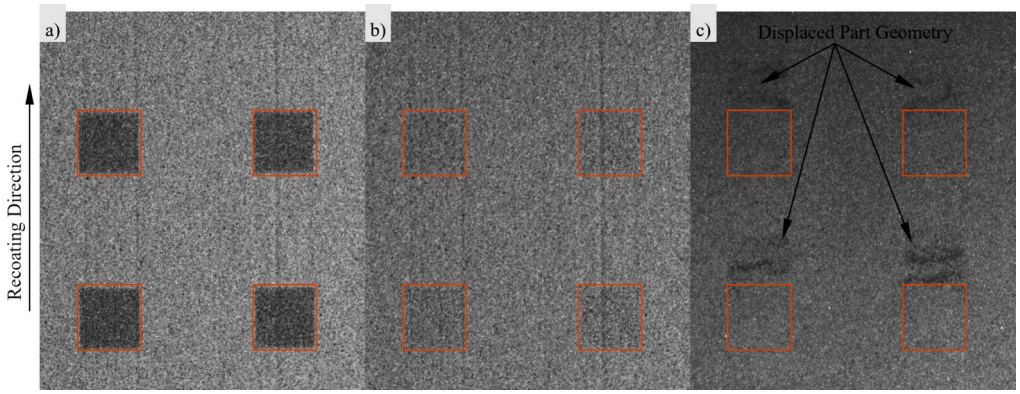

Fig. 21. Camera images of powder bed surface with a) reference layer with printed part, b) recoated layer with 88° blade angle, c) recoated layer with 92° blade angle.

approximately 40°.

The results indicate that roller circumferential speeds below 200 mm/s increase the normal force component, potentially leading to stronger powder bed compaction and higher risk of layer displacement. Circumferential speeds above 200 mm/s show stable and low force ratios. This shows that it is important to consider the relative speed between the recoater and the powder bed with counterclockwise rotating rollers.

The non-linear force decrease confirms the theoretical models of Wang et al. [9] and Nan et al. [4] on the breaking of force chains through rotational movement. The stabilization above 200 mm/s is consistent with the dynamic wall effect described by Chen et al. [7], where the roller acts as a dynamic wall that continuously disrupts force chains. The requirement for rough roller surfaces for particle transport is confirmed by the results and corresponds to the recommendations of Wang et al. [9].

4.2. *Influence of recoating velocity*

For blade recoaters, increasing the recoating velocity from 100 mm/s to 300 mm/s reduces the tangential while the normal force and force magnitude decrease only slightly. The force angle remains unchanged. This can be attributed to the increased momentum of the powder pile at higher velocity: the kinetic energy reduces the force required to move the pile. A comparison of the force differences at the transition from unprinted to printed areas confirms that higher momentum leads to

sharper force transitions at 300 mm/s.

An additional observation is that at 300 mm/s, the recoating force becomes independent of the blade angle, whereas at 100 mm/s it depends on the blade angle investigated. This suggests that a critical velocity threshold exists beyond which the inertia of the powder pile dominates over geometric effects. However, due to technical problems, the full blade angle range could not be investigated at 300 mm/s. This limitation should be acknowledged more explicitly.

These results confirm Phua et al. [15], who concluded that higher recoating velocities lead to a higher-energy system in the powder pile, improving convective particle flow. For layer shifting, the reduced forces at higher recoating velocity suggest a lower risk of layer displacement. However, the sharper force transitions may create localized stress concentrations at printed-area boundaries.

In contrast to blades, roller recoaters show sharply increased forces with higher recoating velocity, particularly the normal force over printed areas. At 300 mm/s recoating speed, forces increase to 21.4 mN/cm. This indicates that the "trapping effect" outweighs the positive inertia effects observed with blades.

At 0 mm/s roller circumferential speed, the recoating velocity has no direct influence on the force, confirming that the particle transport out of the gap plays a decisive role. At high circumferential speeds, forces stabilize but remain higher at 300 mm/s than at 100 mm/s recoating velocity.

For layer shifting, the increase in normal forces with roller recoating velocity is critical. Unlike blades, higher speeds do not reduce recoating forces with rollers. This has direct practical consequences: roller recoaters require careful velocity optimization, balancing throughput against force levels.

4.3. Influence of binder on recoating forces

A force increase of the recoating force was measured at the transition from unprinted to printed areas when binder was present, while a significantly smaller increase was observed in the control case without binder. This indicates that the presence of binder introduces additional mechanical resistance during recoating. It should be noted that binder curing was neither systematically varied nor directly characterized in the present study as interlayer curing leads to deformation of printed parts, also known as curling. Nonetheless, to address the binder drying during the process, the time between binder deposition and recoating was kept constant across the experiments. Possible underlying mechanisms include early-stage chemical reaction between the sodium silicate binder and the cold-curing hardener, capillary bridging between particles and an increase of local stiffness in the printed region. This alters the contact network in front of the recoater in a manner described by the force chain framework.

The measured force increase indicates that previously printed layers experience additional shear load. The binder-induced resistance raises both normal and shear forces that can impact previously printed layers under unfavorable conditions. The force ratio between tangential and normal components provides further insight. For blade recoaters at 88° - 90° tangential forces exceed normal forces. For roller recoaters at low circumferential speeds, normal forces dominate.

This observation is consistent with the CFD-DEM simulations of Li et al. [27], who showed that printed layers are displaced under combined normal and shear forces during recoating. The increasing reaction time of their binder improves its resistance to shear deformation. While their model uses a thermally activated methacrylate binder and our experiments use a cold-curing inorganic system on different time scales, the qualitative principle applies to both. Mechanical resistance of a printed region grows as the binder reaction progresses. The constant process interval between binder deposition and recoating in our experiments places all measurements at a comparable, though uncharacterized, point along this reaction trajectory.

Environmental factors such as air humidity may have contributed to the observed force variability over printed areas between experiments.

The measured force differences at the binder transition are consistent with the simulation results of Parteli et al. and Yao et al. [13,17], who showed that particles cannot rearrange themselves as easily over printed areas, maintaining intact force chains. Blades show higher force differences at inclined angles than at angles close to 90°, which can be interpreted within the force chain compression theory of Wang et al. [9].

4.4. Powder pile growth and recoating distance

The experimental setup in this study maintains a preset amount of powder, uniformly applied on the powder bed. Across all parameter combinations, recoating forces increase with recoating distance due to the continuous growth of the powder pile in front of the recoater. The growing powder pile increases the mass of the material that must be displaced and reorganized at the recoater face, which is reflected in the rising recoating forces. As the pile grows, more force chains form leading to higher net forces on the recoater. Critical part geometries should therefore be positioned at the beginning of the recoating path. In addition, optimized powder dosing that minimizes the pile size while ensuring complete layer coverage could reduce recoating forces. However, this requires a trade-off between process reliability and force reduction, which was not investigated in the present study.

The observed pile growth effect is consistent with the DEM simulations of Wang et al. and Chen et al. [6,10], who showed that force chains form primarily in the powder pile ahead of the recoater.

4.5. Force chain interpretation of load cell signal fluctuations

Beyond the systematic effects of process parameters, the raw force-time signals exhibit pronounced fluctuations that are visible throughout the entire recoating step, as shown in Fig. 12. Wang et al. [9] reported similar behavior in DEM simulations of roller-based powder spreading, where occasional high-force events were observed and attributed to the instability of the spreading process and to force transmission through the powder pile rather than direct recoater-part contact. These fluctuations are qualitatively consistent with the formation and collapse of force chains as described in the DEM literature, where momentary load-bearing particle networks are repeatedly assembled and disrupted as the recoater advances through the powder pile. While the present macroscopic load cell measurements do not resolve individual chain events, the persistent nature of these fluctuations supports interpreting the macroscopic force trends within the established force chain framework. Nevertheless, the oscillations of the measuring system could interfere with the force chain events during the measurement.

4.6. Limitations and transferability

The experiments in this study differ from the simulations and experimental studies in literature in several respects. First, the sand particles have a significantly higher mean diameter compared to typical metal powders, and their grain shape is more irregular. Due to the larger particle size, cohesion effects are negligible in this work, whereas they play a significant role in fine metal powders.

Second, the powder application method differs. Often in commercial printers and experimental setups powder is pre-applied at one end and distributed across the build platform, causing the powder pile to decrease during recoating. In the present experimental setup, powder is uniformly applied and then smoothed, leading to pile growth. As a consequence, segregation effects that are reported for metal AM are not expected here, as only excess particles above the target layer height are removed. The error bars in the measurements reflect the natural variability arising from individual differences in particle packing and inherent stochasticity of granular flow under repeated recoating steps [9,21].

5. Summary and outlook

This work presents an experimental quantification of recoating forces in sand binder jetting, for which experimental data has, to our knowledge, not previously been reported in the literature. The measurements characterize how blade angle, roller circumferential speed, recoating velocity and the transition between unprinted and printed areas affect both the tangential and normal force on the powder bed. The resulting data complements existing DEM-based literature of force chain frameworks with macroscopic experimental measurements and provides a basis for the systematic study of process parameter effects in sand binder jetting.

The recoating forces in sand binder jetting were investigated and determined for various parameter combinations via an innovative setup. The topic is motivated by the problem of layer displacement under unfavorable process parameters. While extensive theoretical simulations and some practical experiments were reported for metal PBF, this work fills an apparent research gap: systematic investigations of recoating forces in sand binder jetting. To the authors' knowledge, this work pioneers an experimental approach to characterizing recoating forces in sand binder jetting under varied process conditions.

With the aid of a specially developed measuring device with a 2-load-cell-measuring cell system, tangential and normal forces were recorded for various recoating parameters. Blade angles of 70°–92°, roller circumferential speeds of 0 mm/s–500 mm/s, recoating velocity of 100 mm/s and 300 mm/s and a layer thickness of 280 µm were systematically investigated. GS14RP sand was used as the material. In addition, the transition from unprinted to printed areas was investigated to analyze different flow properties and the influence of printed parts.

Blade recoaters showed an influence on the tangential force due to the movement effects of the powder pile. The optimum operating range for blade recoaters is between blade angles 88° and 90°. The critical operating range is at blade angles beyond 90°. The base force angle of 20° is achieved with blade recoaters at a blade angle of 90°. Rollers had a stronger influence on the normal force, although the tangential force also had a significant effect. Rollers also cause “trapping effects” in the gap, which is why the roller circumferential speed plays a decisive role. From a roller circumferential speed of 200 mm/s, the recoating forces no longer decrease significantly, which may be linked to the relative speed. Similar trapping effects occur at blade angles beyond 90°. In terms of recoating velocity, blades have a lower influence than rollers. In the case of rollers, the roller circumferential speed is again the decisive factor.

The force differences at transitions from unprinted to printed areas show that the recoating forces could serve as quantitative indicators for possible layer shifts. Especially at higher recoating velocities, blades exhibit lower force differences, which could indicate a lower risk of layer shifts. In the future, recoating forces should be correlated with layer shifts using suitable methods, such as optical measurements and quantitative classification of layer shifts. The applicability of the proposed method must be validated.

Several aspects merit further investigation. The influence of the powder pile size on recoating forces should be quantified, as varying the powder supply would provide data on the relationship between pile volume and force magnitude. Future work should correlate recoating forces with actual layer displacement using suitable optical methods to establish a quantitative relationship for the impact between force magnitude and displacement distance. Additionally, the sensitivity of the measurements to environmental conditions such as ambient humidity should be systematically characterized, as experiments indicated that such factors influence the results. The applicability of the proposed measurement method must be validated across different sand types and binder systems.

CRediT authorship contribution statement

Raphael Burger: Writing – original draft, Visualization, Validation, Software, Resources, Methodology, Investigation, Formal analysis, Data curation, Conceptualization. **Maximilian Mack:** Writing – review & editing, Software, Methodology, Investigation, Data curation. **Veikka Innanen:** Writing – review & editing, Software, Methodology, Investigation, Data curation. **Elodie Donval:** Writing – review & editing, Investigation. **Matti Schneider:** Writing – review & editing, Investigation, Funding acquisition. **Philipp Lechner:** Writing – review & editing, Investigation, Funding acquisition. **Wolfram Volk:** Writing – review & editing, Supervision. **Daniel Günther:** Writing – review & editing, Supervision, Resources, Methodology, Investigation, Funding acquisition, Formal analysis, Conceptualization.

Declaration of competing interest

The authors declare that they have no known competing financial interests or personal relationships that could have appeared to influence the work reported in this paper.

Acknowledgements

Funding by the Deutsche Forschungsgemeinschaft (DFG, German Research Foundation) – 507778349 – is gratefully acknowledged by all the authors. We thank Heiko Andrä and Hannes Grimm-Strele (Flow and Material Simulation, Fraunhofer ITWM Kaiserslautern) for their constructive input, Katja Feßl (Fraunhofer Institute for Casting, Composite and Processing Technology) for the electron microscopy imagery and analysis, and the anonymous reviewers for their constructive comments.

Data availability

Data will be made available on request.

References

[1] P. Erhard, C. Hartmann, R. Li, W. Volk, D. Günther, Advanced procedures for series production with 3D-printed core packages, Int. Metalcast. 17 (4) (2023) 2572–2583, https://doi.org/10.1007/s40962-023-01046-1.
[2] H. Fox, A.B. Kamaraj, D. Drake, Investigating the effect of powder recoater blade material on the mechanical properties of parts manufactured using a powder-bed fusion process, Manuf. Lett. 33 (2022) 561–568, https://doi.org/10.1016/j.mfglet.2022.07.071.
[3] K. Zhao, Z. Su, Z. Ye, W. Cao, J. Pang, X. Wang, Z. Wang, X. Xu, J. Zhu, Review of the types, formation mechanisms, effects, and elimination methods of binder jetting 3D-printing defects, J. Mater. Res. Technol. 27 (2023) 5449–5469, https://doi.org/10.1016/j.jmrt.2023.11.045.
[4] W. Nan, M. Ghadiri, Numerical simulation of powder flow during spreading in additive manufacturing, Powder Technol. 342 (2019) 801–807, https://doi.org/10.1016/j.powtec.2018.10.056.
[5] S. Wu, Y. Yang, Y. Huang, C. Han, J. Chen, Y. Xiao, Y. Li, Di Wang, Study on powder particle behavior in powder spreading with discrete element method and its critical implications for binder jetting additive manufacturing processes, Virtual Phys. Prototyp. 18 (1) (2023) e2158877, https://doi.org/10.1080/17452759.2022.2158877.
[6] H. Chen, Q. Wei, S. Wen, Z. Li, Y. Shi, Flow behavior of powder particles in layering process of selective laser melting: numerical modeling and experimental verification based on discrete element method, Int. J. Mach. Tools Manuf. 123 (2017) 146–159, https://doi.org/10.1016/j.ijmachtools.2017.08.004.
[7] H. Chen, T. Cheng, Z. Li, Q. Wei, W. Yan, Is high-speed powder spreading really unfavourable for the part quality of laser powder bed fusion additive manufacturing? Acta Mater. 231 (2022) 117901 https://doi.org/10.1016/j.actamat.2022.117901.
[8] Q. Chen, E. Juste, M. Lasgorceix, F. Petit, A. Leriche, Binder jetting process with ceramic powders: influence of powder properties and printing parameters, Open Ceram. 9 (2022) 100218, https://doi.org/10.1016/j.oceram.2022.100218.
[9] L. Wang, A. Yu, E. Li, H. Shen, Z. Zhou, Effects of spreader geometry on powder spreading process in powder bed additive manufacturing, Powder Technol. 384 (2021) 211–222, https://doi.org/10.1016/j.powtec.2021.02.022.
[10] L. Wang, Z. Zhou, E. Li, H. Shen, A. Yu, Powder deposition mechanism during powder spreading with different spreader geometries in powder bed fusion additive manufacturing, Powder Technol. 395 (2022) 802–810, https://doi.org/10.1016/j.powtec.2021.10.017.
[11] S. Haeri, Optimisation of blade type spreaders for powder bed preparation in additive manufacturing using DEM simulations, Powder Technol. 321 (2017) 94–104, https://doi.org/10.1016/j.powtec.2017.08.011.

[12] G. Miao, W. Du, Z. Pei, C. Ma, A literature review on powder spreading in additive manufacturing, Addit. Manuf. 58 (2022) 103029, https://doi.org/10.1016/j.addma.2022.103029.
[13] D. Yao, X. An, H. Fu, H. Zhang, X. Yang, Q. Zou, K. Dong, Dynamic investigation on the powder spreading during selective laser melting additive manufacturing, Addit. Manuf. 37 (10) (2021) 101707, https://doi.org/10.1016/j.addma.2020.101707.
[14] J. Zhang, Y. Tan, T. Bao, Y. Xu, X. Xiao, S. Jiang, Discrete element simulation of the effect of roller-spreading parameters on powder-bed density in additive manufacturing, Materials (Basel, Switzerland) 13 (10) (2020), https://doi.org/10.3390/ma13102285.
[15] A. Phua, C. Doblin, P. Owen, C.H. Davies, G.W. Delaney, The effect of recoater geometry and speed on granular convection and size segregation in powder bed fusion, Powder Technol. 394 (2021) 632–644, https://doi.org/10.1016/j.powtec.2021.08.058.
[16] S. Haeri, Y. Wang, O. Ghita, J. Sun, Discrete element simulation and experimental study of powder spreading process in additive manufacturing, Powder Technol. 306 (2016) 45–54, https://doi.org/10.1016/j.powtec.2016.11.002.
[17] E.J. Parteli, T. Pöschel, Particle-based simulation of powder application in additive manufacturing, Powder Technol. 288 (2016) 96–102, https://doi.org/10.1016/j.powtec.2015.10.035.
[18] J. Liu, F. Nicot, W. Zhou, Sustainability of internal structures during shear band forming in 2D granular materials, Powder Technol. 338 (2018) 458–470, https://doi.org/10.1016/j.powtec.2018.07.001.
[19] P. Avrampos, G.-C. Vosniakos, A review of powder deposition in additive manufacturing by powder bed fusion, J. Manuf. Process. 74 (2022) 332–352, https://doi.org/10.1016/j.jmapro.2021.12.021.
[20] M. Massoudi, M.M. Mehrabadi, A continuum model for granular materials: considering dilatancy and the Mohr-Coulomb criterion, Acta Mech. 152 (1–4) (2001) 121–138, https://doi.org/10.1007/BF01176949.
[21] H. Chen, Q. Wei, Y. Zhang, F. Chen, Y. Shi, W. Yan, Powder-spreading mechanisms in powder-bed-based additive manufacturing: experiments and computational modeling, Acta Mater. 179 (2019) 158–171, https://doi.org/10.1016/j.actamat.2019.08.030.
[22] A.L. Maximenko, I.D. Olumor, A.P. Maidaniuk, E.A. Olevsky, Modeling of effect of powder spreading on green body dimensional accuracy in additive manufacturing by binder jetting, Powder Technol. 385 (2021) 60–68, https://doi.org/10.1016/j.powtec.2021.02.070.
[23] H. Miyanaji, M. Orth, J.M. Akbar, L. Yang, Process development for green part printing using binder jetting additive manufacturing, Front. Mech. Eng. 13 (4) (2018) 504–512, https://doi.org/10.1007/s11465-018-0508-8.
[24] S.E. Brika, V. Brailovski, A novel apparatus for the simulation of powder spreading procedures in powder-bed-based additive manufacturing processes: design, calibration, and case study, JMMP 7 (4) (2023) 135, https://doi.org/10.3390/jmmp7040135.
[25] D. Yao, J. Wang, Y. Cai, T. Zhao, X. An, H. Zhang, H. Fu, X. Yang, Q. Zou, L. Wang, Composition regulation of composite materials in laser powder bed fusion additive manufacturing, Powder Technol. 408 (2022) 117795, https://doi.org/10.1016/j.powtec.2022.117795.
[26] E. Donval, M. Schneider, H. Grimm-Strele, M. Godehardt, R. Burger, P. Lechner, D. Günther, H. Andrä, A directional contraction method to model sand-based binder jet 3D printed materials, Int. J. Solids Struct. 312 (2025) 113260, https://doi.org/10.1016/j.ijsolstr.2025.113260.
[27] E. Li, W. Yan, Binder-powder interactions in binder jetting: binder drying, layer shifting, and inter-layer binding, Addit. Manuf. 110 (2025) 104951, https://doi.org/10.1016/j.addma.2025.104951.